Research article

Non-apoptotic regulatory cell death scoring system to predict the clinical outcome and drug choices in breast cancer

Qiwang Zhou [1], Xiaokang Gao [1], Hui Xu, Xuan Lu [*]

Department of Thyroid and Breast Surgery, The Affiliated Hospital of Yangzhou University, Yangzhou University, Yangzhou, 225001, China

ARTICLE INFO

ABSTRACT

Background: Breast cancer (BC), the most common cancer among women globally, has been shown by numerous studies to significantly involve non-apoptotic regulatory cell death (RCD) in its pathogenesis and progression.
Methods: We obtained the RNA sequences and clinical data of BC patients from The Cancer Genome Atlas (TCGA) database for the training set, while datasets GSE96058, GSE86166, and GSE20685 from The Gene Expression Omnibus (GEO) database were utilized as validation cohorts. Initially, we performed non-negative matrix factorization (NMF) clustering analysis on the BC samples from the TCGA database to discern non-apoptotic RCD-related molecular subtypes. To identify prognostically-relevant non-apoptotic RCD genes (NRGs) and construct a prognostic model, we implemented three machine learning algorithms: lasso regression, random forest, and XGBoost analysis. The expression of selected genes was verified using real-time quantitative polymerase chain reaction (RT-qPCR), single-cell RNA-sequencing (scRNA-seq) analysis, and The Human Protein Atlas (HPA) database. The risk signature was evaluated concerning clinical characteristics and drug sensitivity. Furthermore, we developed a nomogram to predict BC patient survival.
Results: The NMF method successfully compartmentalized patients from the TCGA database into three distinct non-apoptotic RCD-related subtypes, with significant variations observed in immune characteristics and prognostic stratification across these subtypes. We identified 5 differentially expressed NRGs used in establishing the risk signature. Patients with different risk groups exhibited distinct clinicopathological features, drug sensitivity, and prognostic outcomes. A nomogram was subsequently developed, incorporating the NRGs-related risk signature, age, T stage, and N stage, to aid clinical decision-making.
Conclusion: We identified a novel NRGs-related risk signature, which was expected to become a potential prognostic marker in BC.

1. Introduction

According to the International Agency for Research on Cancer, breast cancer (BC) has now surpassed lung cancer to become the most prevalent form of malignancy among women worldwide [1]. Despite significant advancements in BC therapies, a fraction of patients still face daunting prognoses due to issues such as drug resistance, recurrence, and metastasis [2,3]. In the era of precision

* Corresponding author.
  E-mail address: 13815820235@163.com (X. Lu).
[1] Qiwang Zhou and Xiaokang Gao contributed equally to this work.

medicine, the need for individualized patient assessment and personalized treatment plans for BC has escalated. However, prevailing prognostic evaluation and treatment stratification for BC primarily hinge on TNM (tumor node and metastasis) staging and molecular subtype [4]. Given the complexity of treatment and the tumor's heterogeneity, there is a pressing need to develop novel high-precision biomarkers for predicting the prognosis of BC patients and guiding treatment.

Contrary to uncontrolled necrosis, regulatory cell death (RCD) represents a meticulously orchestrated cell death mechanism, steered by gene expression events [5]. Apoptosis, a well-studied RCD form, is the main target of current anti-cancer chemotherapeutic agents [6]. However, tumors can circumvent apoptosis through strategies such as overexpression of anti-apoptotic proteins, leading to resistance to multiple chemotherapy drugs [7]. Recently, numerous novel non-apoptotic RCD forms have emerged, including autophagy, pyroptosis, ferroptosis, necroptosis, cuproptosis, and disulfidptosis, offering a rich array of alternative therapeutic targets [8,9]. Significant advancements have been made in therapies targeting non-apoptotic RCD in BC. For instance, phloretin, a dihydrochalcone flavonoid compound, has been demonstrated to counteract tamoxifen resistance by modulating autophagy in triple-negative BC (TNBC) cells (Chen et al., 2021) [10]. Additionally, Zeng et al. have engineered a nanohybrid capable of inducing ferroptosis, thereby enhancing radiotherapy efficacy and improving TNBC treatment outcomes [11]. Notably, mounting evidence underscores significant crosstalk and cross-regulation amongst these signaling pathways [12–14]. Despite this, the bulk of current research remains centered on elucidating the role of specific types of non-apoptotic RCD in the progression and prognosis of BC.

In the present study, we conducted an exhaustive analysis of the expression of non-apoptotic RCD genes (NRGs) in BC. Utilizing the Cancer Genome Atlas (TCGA) database, we discerned three distinct subgroups of non-apoptotic RCD in BC. Moreover, we constructed a robust risk signature, composed of 5 NRGs, that prognosticates the outcome in BC. The cellular distribution and expression levels of these risk gene signatures were further validated by employing real-time quantitative polymerase chain reaction (RT-qPCR), single-cell RNA-sequencing (scRNA-seq) analysis, and The Human Protein Atlas (HPA) database. We also explored the disparities in clinical characteristics and drug sensitivity among the various risk cohorts. Collectively, our findings underscore the functional relevance of the NRGs-related risk signature and uncover a potential prognostic biomarker for BC.

2. Materials and methods

2.1. Data acquisition

RNA expression data and clinicopathological information for BC patients were extracted from the TCGA database. Additionally, three relevant datasets (GSE96058, GSE20685, and GSE86166) were retrieved from the Gene Expression Omnibus (GEO) database. To address potential batch effects, we implemented the "ComBat" function from the "sva" R package.

We sourced autophagy-related and ferroptosis-related genes from the GeneCards database, while pyroptosis-related, necroptosis-related, and cuproptosis-related genes were acquired from the Gene Set Enrichment Analysis (GSEA) website and previous literature [15–21]. Additionally, we collected 16 disulfidptosis-related genes from a recent study by Liu et al. [22]. A comprehensive list of these NRGs is provided in Supplementary Table S1.

2.2. Identification of non-apoptotic RCD related subtypes

The "limma" R package was utilized to identify differentially expressed NRGs between normal and tumor samples within the TCGA-BRCA dataset. Subsequent to this, the identified differentially expressed genes (DEGs) were subjected to nonnegative matrix factorization (NMF) clustering. The optimal number of clusters was determined to be k = 3, ascertained through the evaluation of the cophenetic coefficient, contour, and sample size. Principal component analysis (PCA) was utilized to validate the robustness and reliability of the non-apoptotic RCD-related subtypes.

To assess variations in the tumor microenvironment (TME) across different molecular subtypes, the single sample gene set enrichment analysis (ssGSEA) method from the "GSVA" R package and the ESTIMATE algorithm were employed. Moreover, gene set enrichment analysis (GSEA) was performed on patients with diverse molecular subtypes using the "clusterprofiler" R package.

2.3. Construction and validation of the risk model

We utilized the "limma" R package to identify DEGs across diverse molecular subtypes. Furthermore, we investigate whether these DEGs exhibited expression discrepancies between normal and tumor samples within the TCGA-BRCA and GSE65194 datasets. The criteria for significance were set as an absolute log2 fold change (FC) greater than 1 and a false discovery rate (FDR) less than 0.05.

To circumvent potential model overfitting, we integrated three machine learning algorithms, namely lasso regression, random forest (RF), and XGBoost analysis, to construct a more robust predictive model. The risk score for each patient in both the modeling set and validation set was calculated using this model. Subsequently, patients were stratified into high- and low-risk groups based on the median risk score. The accuracy of the risk model was then evaluated using Kaplan-Meier (KM) survival curves, receiver operating characteristic (ROC) curves, and risk score distribution plots.

2.4. RT-PCR analysis

The MCF-10A and T47D cell lines, procured from Procell Life Science and Technology Co., Ltd, were cultured under a humidified atmosphere at 37 °C with 5 % CO_2. For RNA extraction, cells were expanded in suitable culture dishes until they achieved

approximately 80 % confluency. Total RNA was extracted using TRIzol reagent, strictly following the manufacturer's recommendations. The quality and quantity of the resultant RNA samples were evaluated using a NanoDrop spectrophotometer and gel electrophoresis. GAPDH was used as endogenous control. The sequences of the primers utilized are provided in Supplementary Table S2.

2.5. scRNA-seq data processing

ScRNA-seq data was procured from the GSE161529 dataset, encompassing 32 samples of breast carcinoma and 13 samples of non-neoplastic breast tissue [23]. Pre-processing measures included ensuring expression of each gene in a minimum of three cells, maintaining the gene expression per cell within the range of 300–7000, and limiting the mitochondrial gene content to less than 15 %. The "harmony" R packages was employed for the mitigation of batch effects among samples, followed by dimension reduction via the UMAP method to delineate the cell clusters.

By leveraging the CellMarker database, we undertook manual annotation to stratify all cell clusters into distinct subgroups: epithelial cells (EPCAM, KRT8, and KRT17), fibroblasts (COL3A1 and PDGFRA), pericytes (RGS5), endothelial cells (VWF, PECAM1, CD36, CDH5, and SELE), T cells (CD3D and CD2), B cells (MS4A1 and CD79A), and Myeloid cells (CD68, CD14, CD163, and CSF1R) [24].

2.6. Construction and validation of the prognostic nomogram

Ultimately, we executed univariate and multivariate analyses to validate the independent prognostic value of the NRGs-related risk signature. Following this, we formulated a prognostic nomogram for the prediction of 3- and 5-year OS rates in BC patients. The performance of the model was evaluated through a variety of methods, including the concordance index (*C*-index), ROC curves, calibration curves, and decision curve analysis (DCA).

2.7. Statistical analysis

The data were processed, analyzed, and presented utilizing R software (version 4.1.0). A two-tailed *P*-value of less than 0.05 was deemed to denote statistical significance.
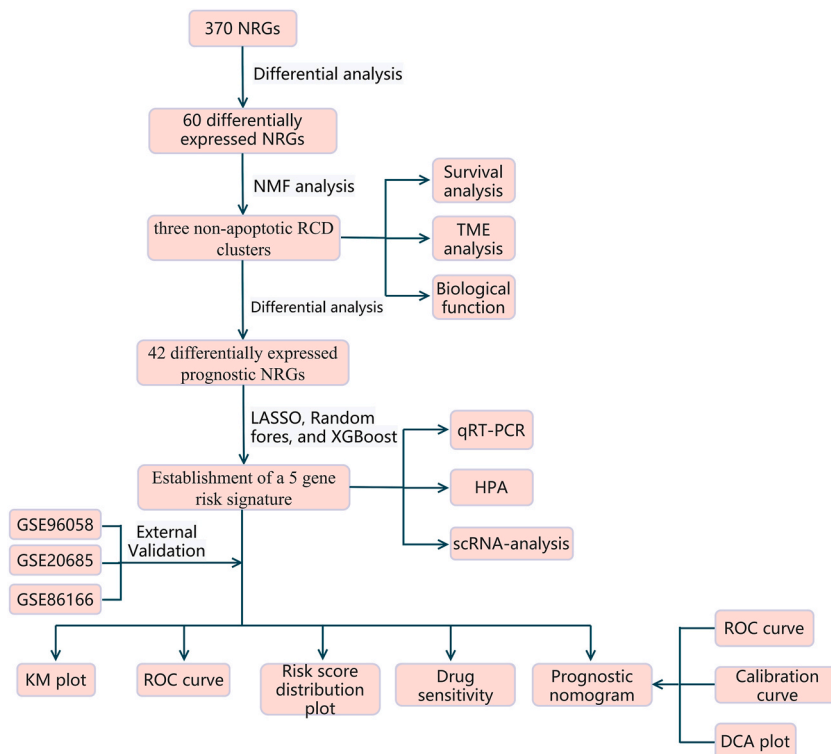

Fig. 1. The flow chart of this study.

3. Results

3.1. Identification of distinct non-apoptotic RCD associated subtypes

The schematic representation of the entire study workflow is delineated in Fig. 1. From the TCGA-BRCA dataset, we collated 941 tumor tissue samples, along with their concomitant clinical data. Additionally, we also included 95 normal tissue samples for comparison. The differential expression analysis of NRGs revealed 60 distinct genes, out of which 37 exhibited upregulation in tumor tissues Fig. 2A.

Employing the NMF algorithm for sample clustering based on the differential NRG expression, we discerned the formation of three distinct clusters (C1, C2, and C3) when the number of clusters (k) was set to 3, as inferred from covariance and residual sum of squares
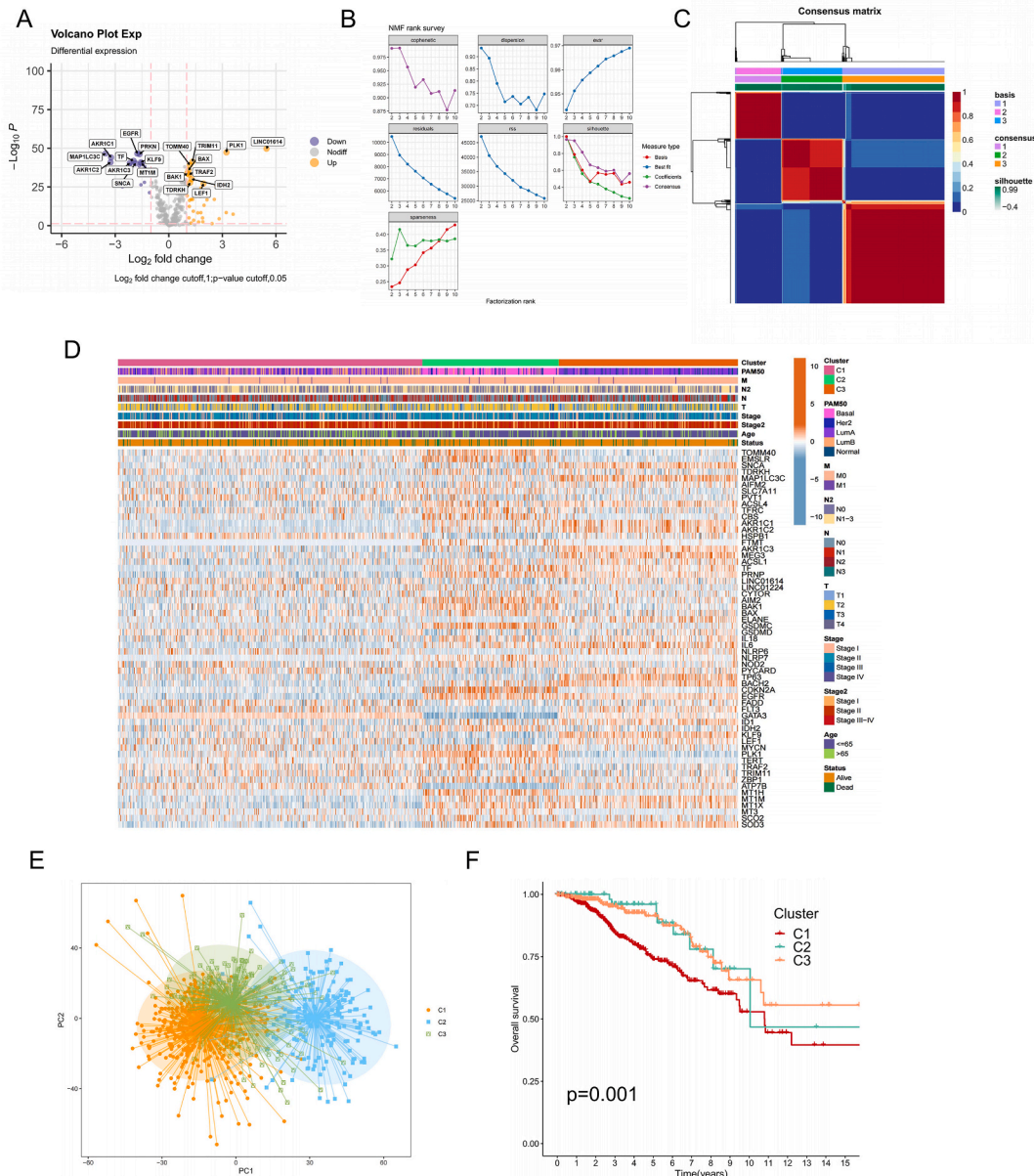
Fig. 2. Identification of three distinct non-apoptotic RCD-related molecular subtypes in BC via NMF analysis. (A) Volcano plot illustrating differentially expressed NRGs between cancerous and normal tissues. (B) Determination of factorization rank for k ranging from 2 to 10. (C) Cluster mapping based on the NMF algorithm. (D) Heatmap representation of the NRGs' expression patterns across distinct molecular subtypes. (E) PCA scatter plot substantiating the classification into three non-apoptotic RCD molecular subtypes. (F) KM survival curves for the three identified clusters within the TCGA-BRCA dataset.

(RSS) analyses (Fig. 2B). Further, the consensus matrix heatmap for k = 3 manifested clearer demarcation compared to other cluster numbers, underscoring the optimal cluster identification (Fig. 2C). The differential NRG expression across these three molecular subtypes is depicted in Fig. 2D. The PCA results corroborated the distinct distribution patterns of the three clusters (Fig. 2E). Kaplan-Meier survival analyses underscored that patients within the C2 and C3 clusters exhibited significantly superior prognostic outcomes compared to those in the C1 cluster, emphasizing the clinical relevance of these molecular subtypes (Fig. 2F).

3.2. Diverse molecular subtypes exhibit varied TME and biological functions

Recent studies have underscored the pivotal role of non-apoptotic RCD in myriad facets of immune cell biology, encompassing their survival, differentiation, activation, and migratory behaviors [25–27]. In the present investigation, we leveraged the ssGSEA algorithm to probe the infiltration dynamics of immune cells across the three non-apoptotic RCD subtypes. Significantly, we discerned pronounced variations among discrete immune cell subpopulations, such as activated B cells, activated CD4$^+$ T cells, activated CD8$^+$ T cells, and natural killer T cells, with a preponderance in the C2 cluster (Fig. 3A). In alignment with the ssGSEA findings, the C2 cluster manifested the highest immune score as per the ESTIMATE algorithm, whereas the C1 cluster demonstrated the lowest (Fig. 3B). These observations shed light on the intricate dynamics of immune cells linked with non-apoptotic RCD subtypes. We further noted significant disparities in tumor purity and stromal scores among the distinct molecular subtypes (Fig. 3C–F). The C1 cluster displayed elevated tumor purity, potentially contributing to a poorer prognosis (Fig. 3C). Concurrently, the C2 cluster exhibited a significantly higher stromal score compared to the C1 and C3 clusters (Fig. 3D–F). Moreover, GSEA findings, utilizing the Hallmark pathway database, revealed significant variations in enrichment patterns across different traits (Fig. 3G–I).
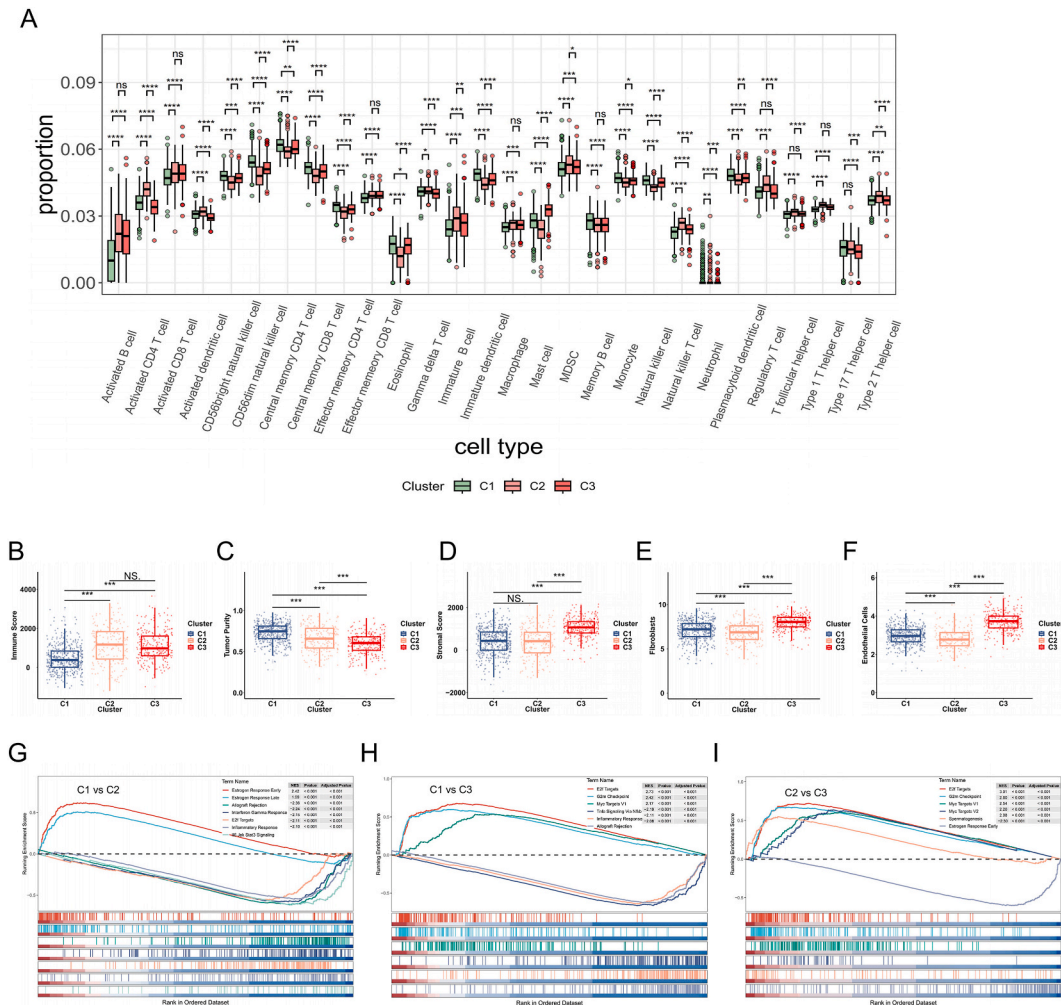

Fig. 3. Assessment of TME and biological processes. (A) ssGSEA analysis was employed to evaluate the infiltration levels of 28 immune cells across the three identified clusters. (B–F) The ESTIMATE analysis was utilized to evaluate the immune score, tumor purity, and stromal score in distinct molecular subtypes. (G–I) GSEA was employed for functional enrichment analysis.

3.3. Construction prognostic signature for NRGs

Upon discerning the disparities among the three non-apoptotic RCD clusters, our subsequent investigation focused on identifying prognostic markers intertwined with NRGs. We identified 8248 DEGs between the C1 and C2 clusters, 8802 DEGs between the C1 and C3 clusters, and 5385 DEGs between the C2 and C3 clusters. After intersecting these genes, we further selected those exhibiting differential expression between normal and tumor samples in both the TCGA-BRCA and GSE65194 datasets for the construction of an NRGs-related risk signature (Fig. 4A). Following this, we utilized univariate Cox regression analysis and identified 42 NRGs significantly correlated with the prognosis of BC patients (Fig. 4B). To mitigate model overfitting, we employed three machine-learning methodologies for variable selection, including lasso regression, RF, and XGBoost analysis (Fig. 4C–F). Consequently, we identified five core NRGs (ARID5A, TFPI2, SDC1, CEMIP, SIAH2) in BC as prognostic indicators (Fig. 4G). The resulting risk scoring formula was as follows: Risk score = (0.152 * SDC1 expression) + (0.046 * CEMIP expression) - (0.326 * ARID5A expression) - (0.149 * TFPI2 expression) - (0.146 * SIAH2 expression).

3.4. Assessment of the performance of the NRGs-related model

Risk scores were computed for each sample in the training set and the three validation sets utilizing the risk score formula.
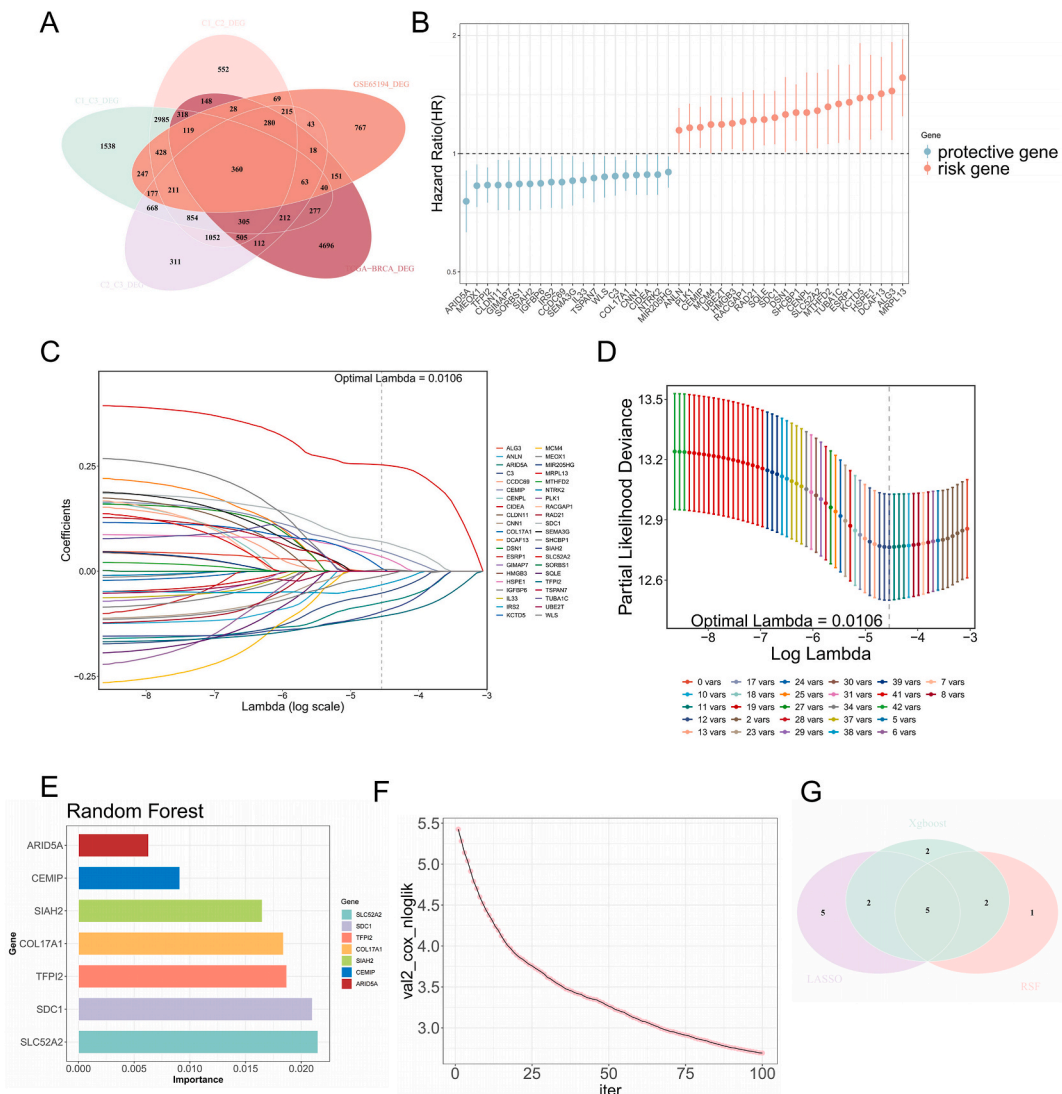
Fig. 4. Construction of risk features associated with non-apoptotic RCD. (A) Venn diagram representation. (B) Implementation of Univariate Cox regression analysis for the identification of prognosis-related OS genes. (C–D) Application of LASSO regression analysis. (E) Utilization of the Random Forest algorithm for analysis. (F) Execution of XGBoost analysis. (G) The Venn diagram illustrates the intersections of results derived from different machine learning algorithms.

Following this, patients were categorized into high-risk and low-risk groups using the median risk score as the demarcation. Within the TCGA-BRCA training set, the KM survival curves distinctly showcased a marked difference in prognosis between the high-risk and low-risk groups (Fig. 5A). The robust predictive proficiency of the model was underscored by the ROC curves (Fig. 5B). Moreover, the distribution of risk scores is visually represented in Fig. 5C, emphatically illustrating that samples with elevated risk scores significantly correlate with shorter survival times in contrast to those with lower risk scores. Analogous results were obtained when identical methodologies were applied to the validation sets (Fig. S1). We investigated the association between the risk score and clinicopathological characteristics to assess the predictive precision of the risk scores for these traits. Patients classified into the high-risk group demonstrated significantly advanced tumor stages and histological grades in comparison to those allocated to the low-risk group. Furthermore, patients classified as Basal and Her2 subtypes under the PAM50 classification exhibited higher risk scores than other subtypes (Fig. 5D–K).

3.5. Drug sensitivity analysis

To establish a more robust association between the risk signature and clinical application, we utilized the "oncoPredict" R package to appraise the responsiveness of patients stratified into high-risk and low-risk groups to widely administered endocrine and chemotherapy agents for BC. Drug sensitivity and therapeutic efficacy were evaluated based on IC50 values, denoting the median 50 % inhibitory concentration. The outcomes disclosed that patients in the low-risk group manifested enhanced sensitivity to cyclophosphamide, docetaxel, epirubicin, gemcitabine, paclitaxel, palbociclib, tamoxifen, and olaparib treatments, as evidenced by diminished IC50 values (Fig. 6A–H). These insights may provide implications for directing the choice of pharmacological therapy for BC patients.

3.6. Validation of the expression levels of selected NRGs

We evaluated the expression of risk signature genes in a BC cell line, T47D, and a normal cell line, MCF10A, employing RT-qPCR. The expression levels of CEMIP, SIAH2, SDC1, and TFPI2 were elevated, while those of ARID5A were attenuated in T47D relative to MCF10A (Fig. 7A–E). Moreover, we investigated the protein expression levels of these genes in BC patients utilizing the HPA database. The protein-level outcomes of ARID5A, CEMIP, SIAH2 and TFPI2 were in alignment with our PCR results. Unfortunately, data pertaining to CEMIP expression were not available in the HPA database (Fig. 7F).
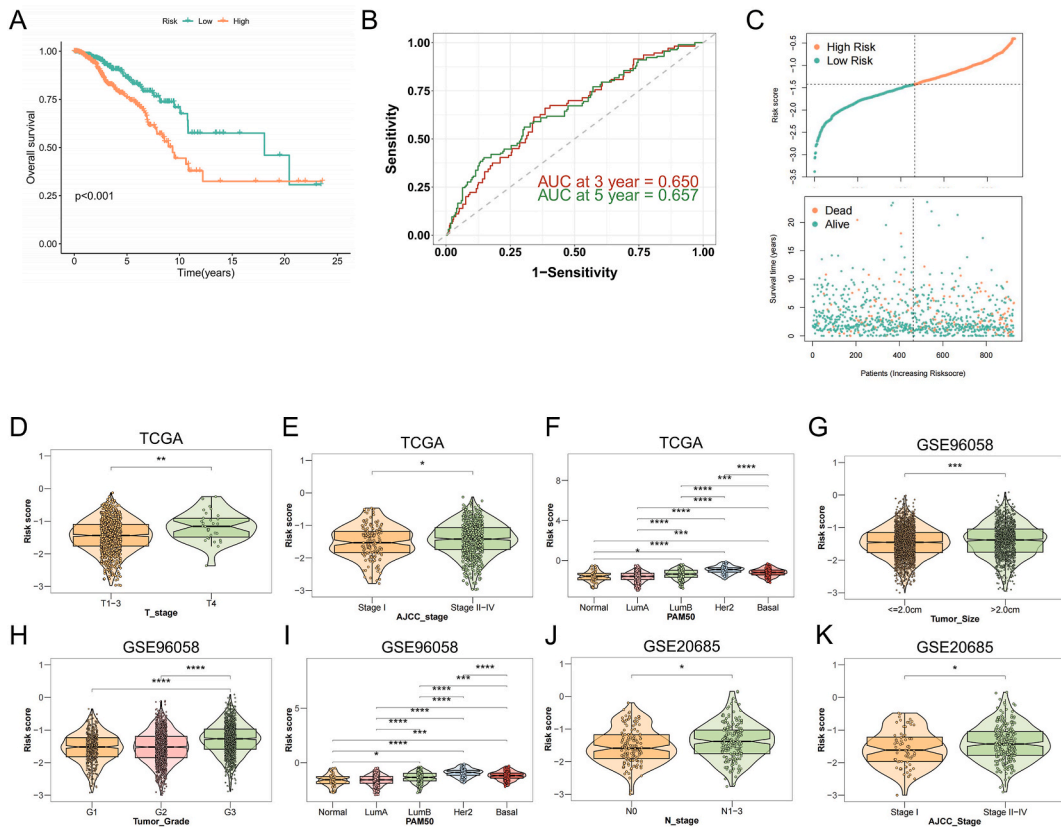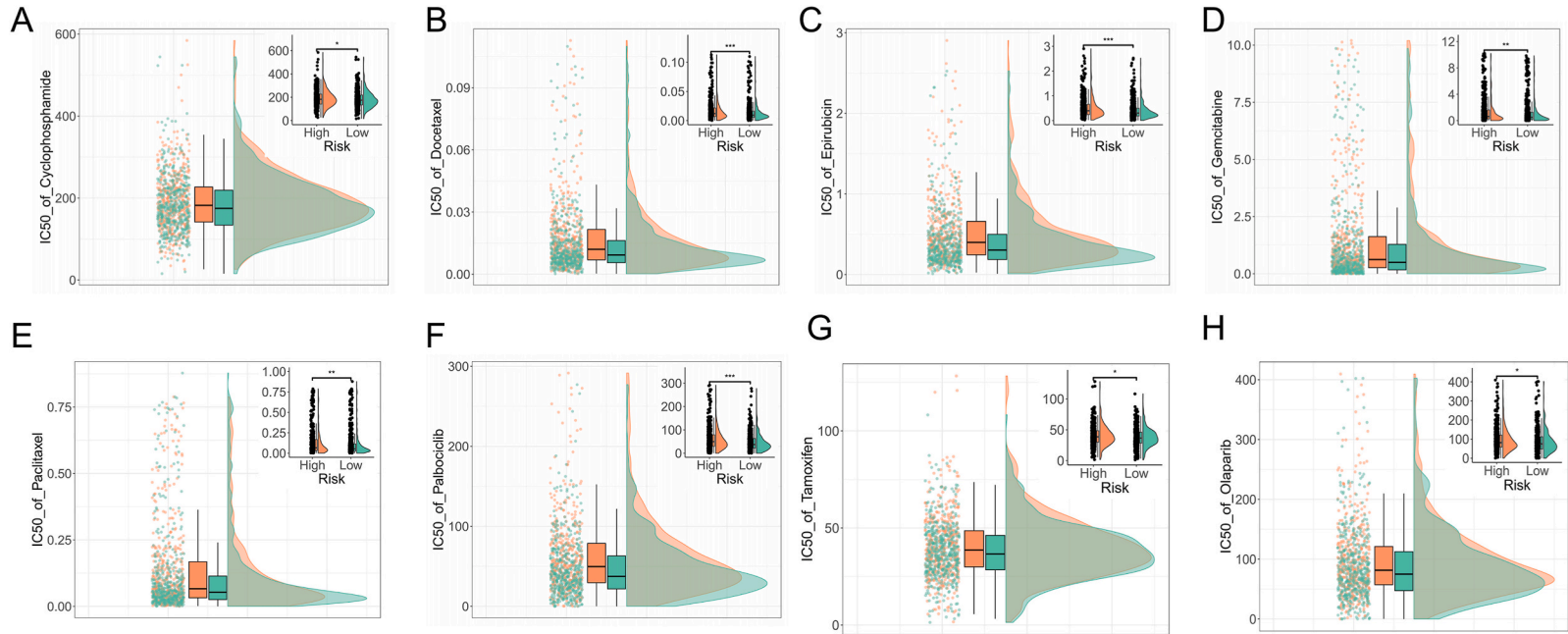

Fig. 5. Clinical correlation and survival analysis. (A–C) KM survival curves, ROC curves, and risk distribution plots in TCGA-BRCA database. (D–K) Correlation analysis between risk score and clinicopathological characteristics.

Fig. 6. The drug sensitivity analysis reveals that the risk score correlates with the treatment sensitivity of cyclophosphamide (A), docetaxel (B), epirubicin (C), gemcitabine (D), paclitaxel (E), palbociclib (F), tamoxifen (G), and olaparib (H).

8

3.7. ScRNA-seq analysis

Upon manual annotation of the single-cell sequencing dataset GSE161529, we distinguished seven cell types, comprising epithelial cells, fibroblasts, pericytes, endothelial cells, T cells, B cells, and myeloid cells (Fig. 8A–B). Following this, we explored the cellular distribution of the five genes implicated in the construction of the risk score. Our observations disclosed that ARID5A was predominantly expressed in epithelial cells, fibroblasts, and endothelial cells. SIAH2 and SDC1 were primarily manifest in epithelial cells, while TFPI2 was chiefly discerned in endothelial cells. Regrettably, CEMIP expression was not identifiable in any of these cell types (Fig. 8C).

3.8. Nomogram construction and validation

The independent prognostic significance of the NRGs-related risk signature was validated via univariate and multivariate Cox regression analyses utilizing the TCGA database (Fig. 9A–B). In light of the findings from the multivariate Cox regression analysis, a nomogram was constructed, amalgamating age, T-stage, N-stage, and the NRGs-related risk score, to foretell the likelihood of OS at 3 and 5 years for BC patients. As portrayed in Fig. 9C, for a 68-year-old female BC patient at stage T1N0, the risk score amounts to 0.5, resulting in an aggregate risk score of 280. The anticipated 3-year and 5-year OS, as delineated in the nomogram, are approximately 84.8 % and 73.4 %, respectively. Various evaluation methodologies, encompassing the ROC curve, calibration curve, and DCA plots, underscored the exceptional predictive prowess of the nomogram (Fig. 9D–G). Comprehensive clinical data for patients in the GSE96058 and GSE86166 datasets were not accessible; hence, we elected to affirm the predictive precision of the model exclusively within the independent validation set GSE20685 (Fig. S2).

4. Discussion

Apoptosis, recognized as the first form of RCD to be identified, was once deemed to be the principal mechanism influencing the survival of cancer cells. Nevertheless, the effectiveness of drugs targeting apoptosis in oncological treatment appears to be thwarted by the advent of drug resistance and immune evasion [28,29]. With the progressive elucidation of cell death mechanisms, an escalating number of novel non-apoptotic RCDs have been discovered, offering new opportunities for therapeutic intervention [30]. A plethora of studies have consistently underscored the complex interplay among diverse non-apoptotic regulated cell death signaling pathways, collectively orchestrating the cell death process [12–14]. However, hitherto, there persists a dearth of research integrating non-apoptotic RCD for the systematic and comprehensive analysis of its prognostic and therapeutic implications in BC.

In the present investigation, we encompassed six types of non-apoptotic RCD, namely apoptosis, ferroptosis, necroptosis, pyroptosis, along with the recently identified cuproptosis and disulfidptosis. By scrutinizing the expression profiles of NRGs, we harnessed
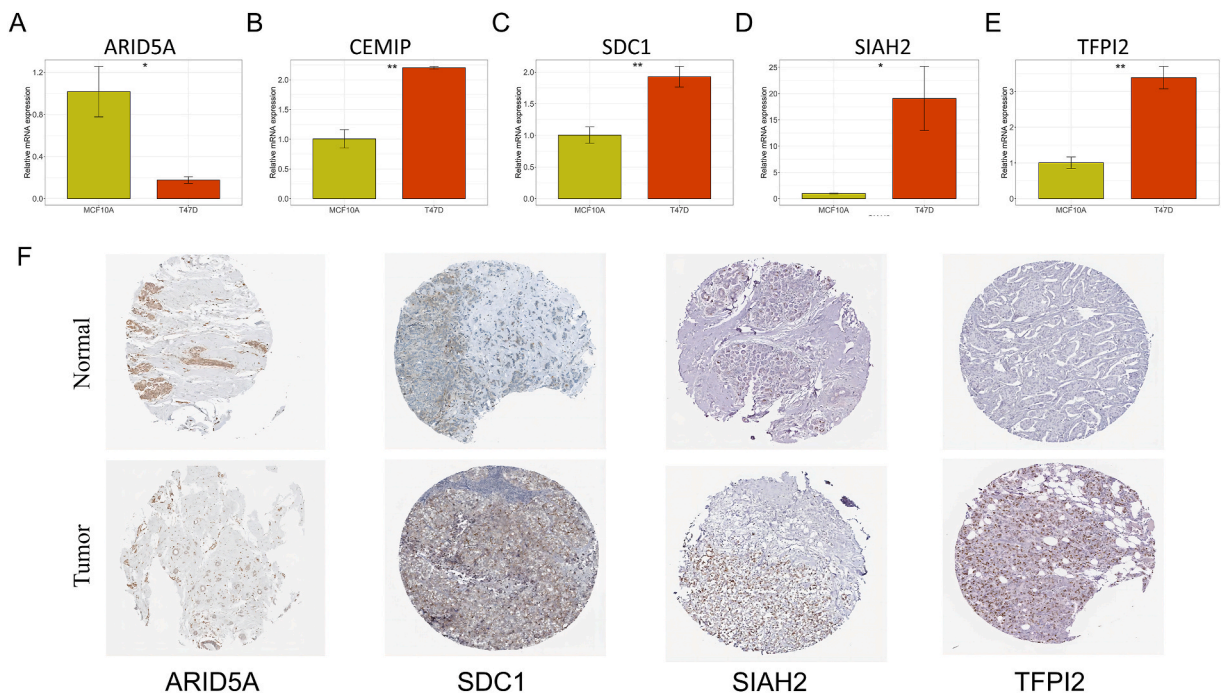

Fig. 7. (A–E) Evaluation of mRNA levels of NRGs in a BC cell line (T47D) and a normal cell line (MCF10A) ascertained by RT-qPCR. (F) Determination of protein levels utilizing data from The Human Protein Atlas (HPA) database.
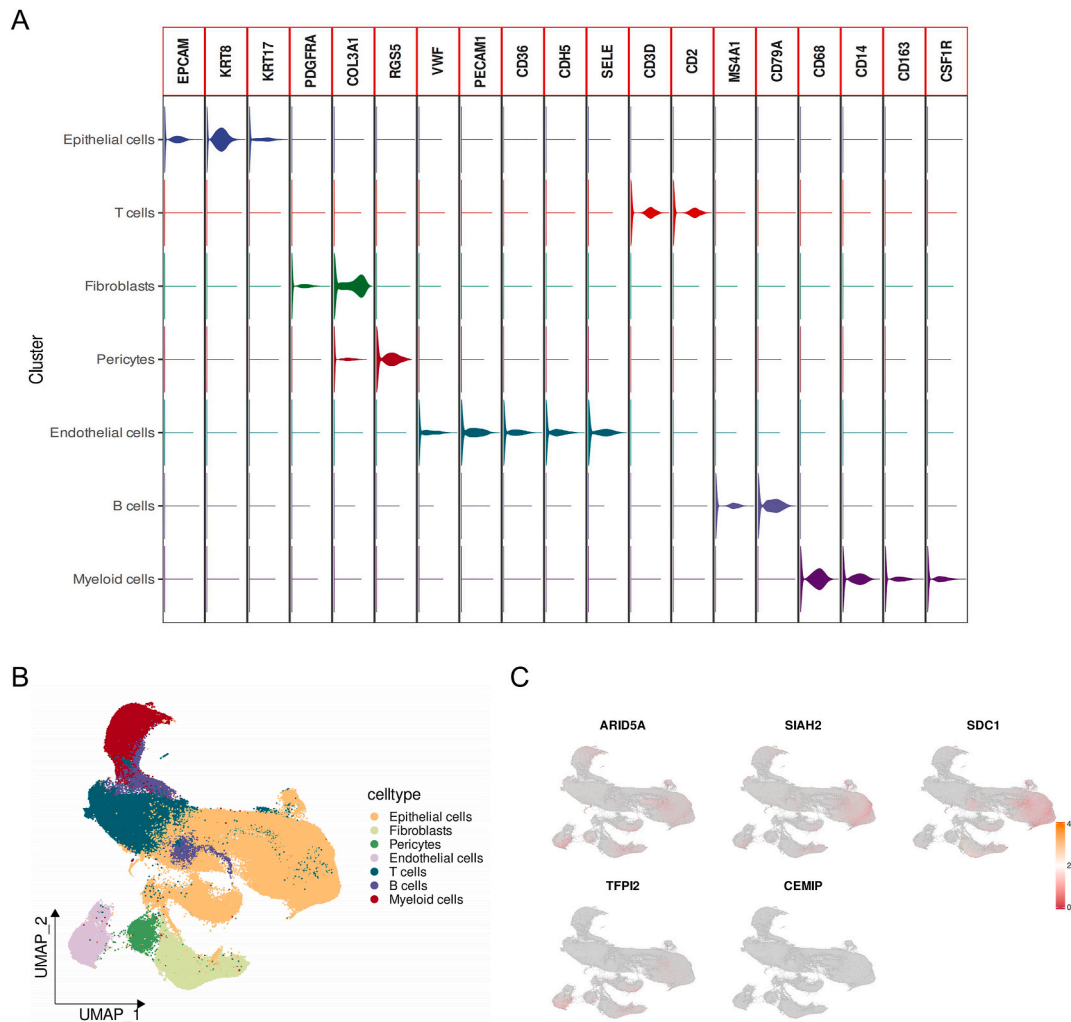
Fig. 8. (A) Violin plot for differential expression levels of marker genes across distinct cell types. (B) UMAP plot of seven cell types. (C) UMAP plot visualization of the distribution of 5 NRGs.

the NMF algorithm to categorize patients in the TCGA-BRCA cohort into three discrete clusters, designated as C1, C2, and C3. We discerned substantial variations in immune cell infiltration, matrix score, and prognosis among these patient clusters. To precisely assess the prognostic risk of non-apoptotic RCD in BC, we devised a 5-gene risk score utilizing machine learning analysis. This risk signature exhibited potent predictive efficacy in both the training set and the three validation sets, thereby underscoring its robustness.

ARID5A, an essential component of the ARID protein family, significantly modulates a wide array of cellular processes, including invasion, metastasis, epithelial-to-mesenchymal transition, and immune evasion [31]. Wang et al. reported an improved prognostic outcome in BC patients exhibiting elevated ARID5A expression, which is consistent with our own findings [32]. TFPI2, a serine proteinase inhibitor, is well-known for its ability to suppress tumor metastasis in different types of cancer cells [33]. For instance, Luo et al. confirmed that overexpression of TFPI2 effectively mitigated proliferation and invasion in Glioblastoma Multiforme (GBM) cells [34]. Comparable conclusions have been drawn by Zhao and Prakasha within the context of BC and fibrosarcoma, respectively [35, 36]. The role of SIAH2 proteins in BC continues to be a subject of debate. Confalonieri and Maurice reported a relatively extended survival period in BC patients expressing high levels of SIAH2 [37]. Christina et al. proposed that SIAH2 loss triggers vascular normalization, thereby amplifying the effectiveness of chemotherapy in BC patients [38]. In contrast, Adam et al. suggested that SIAH2 enhances the migration and invasion of BC cells [39]. Our study noted an escalation in SIAH2 expression in BC, with patients demonstrating high SIAH2 expression presenting a more favorable prognosis. The intricate regulatory mechanisms of SIAH2 in BC warrant further investigation. SDC1, a key cell surface heparan sulfate proteoglycan, serves as a coreceptor for an array of heparin-binding growth factors and engages with multiple extracellular matrix molecules [40]. Numerous studies consistently demonstrate that an upsurge in SDC1 expression in breast carcinomas is linked with a worse prognosis and an aggressive phenotype in BC [41,42]. Moreover, Martin et al. provided evidence that SDC1 expression level could be utilized as a predictive marker for the efficacy of neoadjuvant therapy in BC patients [43]. CEMIP, a protein implicated in the Wnt pathway, has been identified to activate
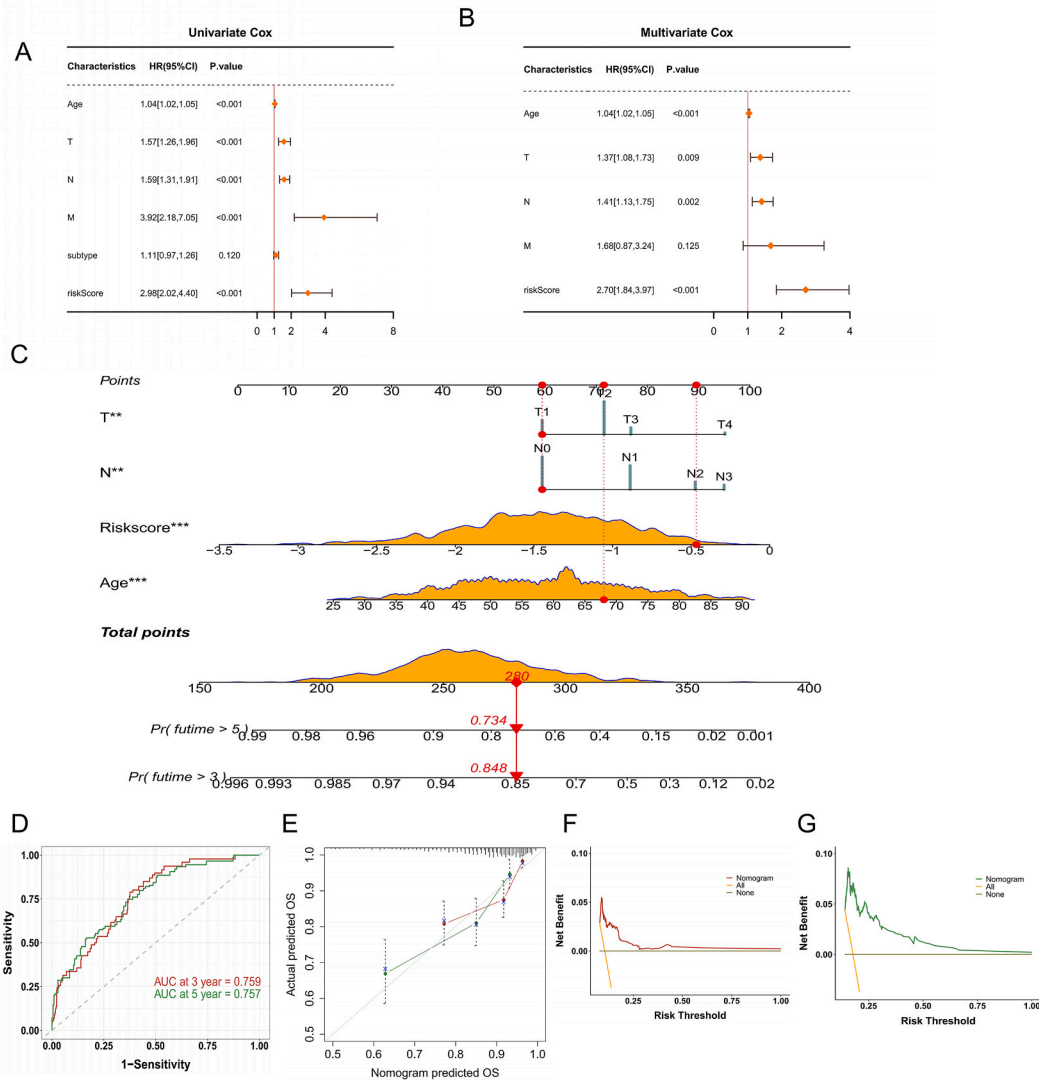
Fig. 9. Construction and Validation of Nomogram. (A–B) Univariate and multivariate Cox regression analyses of risk score in conjunction with clinicopathological attributes. (C) Employment of the nomogram for prognostication of 3- and 5-year OS probabilities in BC patients. (D) Quantification of area under the ROC curves for prognostication of 3- and 5-year survival in TCGA-BRCA cohorts. (E) Calibration plots for the nomogram. (F–G) DCA of 3- and 5-year OS for patients in TCGA.

the STAT3 pathway, thereby fostering cell proliferation and migration in BC [44]. Moreover, CEMIP can facilitate the colonization of BC cells in brain metastases via the release of exosomes [45]. In line with our findings, a study spearheaded by Xue et al. revealed that BC patients with high CEMIP expression levels have a comparatively unfavorable prognosis [46].

This study, however, is not without its limitations. Primarily, it is crucial to underscore that our research is retrospective, hence the devised risk score warrants validation in a prospective study encompassing a larger patient cohort. Additionally, our deductions are predominantly confined to bioinformatic analysis, necessitating further in vitro and in vivo experimentation in ensuing research.

In conclusion, we have successfully devised an innovative scoring algorithm for non-apoptotic RCD that proficiently segregates BC patients based on risk and prognosticates their clinical outcomes. This scoring system presents a valuable tool for guiding clinical treatment decisions. Moreover, we have developed a predictive nomogram model that augments the precision of prognostic prediction for BC patients.

Ethics approval

Since all the data used in the current study was available online, and no individual patient was involved, the IRB (Institutional Review Board) review was exempted.

Data availability statement

All data can be requests from correspondence authors.

CRediT authorship contribution statement

Qiwang Zhou: Writing – review & editing, Writing – original draft, Validation, Software, Resources, Project administration, Methodology, Investigation, Formal analysis, Data curation. **Xiaokang Gao:** Visualization, Validation, Methodology, Formal analysis, Data curation. **Hui Xu:** Visualization, Validation, Methodology, Formal analysis, Data curation. **Xuan Lu:** Supervision, Funding acquisition, Formal analysis, Conceptualization.

Declaration of competing interest

The authors declare that they have no known competing financial interests or personal relationships that could have appeared to influence the work reported in this paper.

Appendix A. Supplementary data

Supplementary data to this article can be found online at https://doi.org/10.1016/j.heliyon.2024.e31342.

References

[1] H. Sung, J. Ferlay, R.L. Siegel, et al., Global cancer statistics 2020: GLOBOCAN estimates of incidence and mortality worldwide for 36 cancers in 185 countries, CA A Cancer J. Clin. 71 (3) (2021) 209–249, https://doi.org/10.3322/caac.21660.
[2] M. Fillon, Breast cancer recurrence risk can remain for 10 to 32 years, CA A Cancer J. Clin. 72 (3) (2022) 197–199, https://doi.org/10.3322/caac.21724.
[3] E. Nolan, G.J. Lindeman, J.E. Visvader, Deciphering breast cancer: from biology to the clinic, Cell 186 (8) (2023) 1708–1728, https://doi.org/10.1016/j.cell.2023.01.040.
[4] M.T. Phung, Tin S. Tin, J.M. Elwood, Prognostic models for breast cancer: a systematic review, BMC Cancer 19 (1) (2019) 230, https://doi.org/10.1186/s12885-019-5442-6.
[5] A. Ashkenazi, G. Salvesen, Regulated cell death: signaling and mechanisms, Annu. Rev. Cell Dev. Biol. 30 (2014) 337–356, https://doi.org/10.1146/annurev-cellbio-100913-013226.
[6] L. Zhang, Z. Lu, X. Zhao, Targeting Bcl-2 for cancer therapy, Biochim. Biophys. Acta Rev. Canc 1876 (1) (2021) 188569, https://doi.org/10.1016/j.bbcan.2021.188569.
[7] B.A. Carneiro, W.S. El-Deiry, Targeting apoptosis in cancer therapy, Nat. Rev. Clin. Oncol. 17 (7) (2020) 395–417, https://doi.org/10.1038/s41571-020-0341-y.
[8] X. Tong, R. Tang, M. Xiao, et al., Targeting cell death pathways for cancer therapy: recent developments in necroptosis, pyroptosis, ferroptosis, and cuproptosis research, J. Hematol. Oncol. 15 (1) (2022) 174, https://doi.org/10.1186/s13045-022-01392-3.
[9] J. Lin, S. Sun, K. Zhao, et al., Oncolytic Parapoxvirus induces Gasdermin E-mediated pyroptosis and activates antitumor immunity, Nat. Commun. 14 (1) (2023) 224, https://doi.org/10.1038/s41467-023-35917-2.
[10] M. Chen, V. Gowd, M. Wang, F. Chen, K.W. Cheng, The apple dihydrochalcone phloretin suppresses growth and improves chemosensitivity of breast cancer cells via inhibition of cytoprotective autophagy, Food Funct. 12 (1) (2021) 177–190, https://doi.org/10.1039/d0fo02362k.
[11] L. Zeng, S. Ding, Y. Cao, et al., A MOF-based potent ferroptosis inducer for enhanced radiotherapy of triple negative breast cancer, ACS Nano 17 (14) (2023) 13195–13210, https://doi.org/10.1021/acsnano.3c00048.
[12] C. Wu, L. Zhou, H. Yuan, S. Wu, Interconnections among major forms of regulated cell death, Apoptosis 25 (9–10) (2020) 616–624, https://doi.org/10.1007/s10495-020-01632-2.
[13] Y. Bai, X. Liu, X. Qi, et al., PDIA6 modulates apoptosis and autophagy of non-small cell lung cancer cells via the MAP4K1/JNK signaling pathway, EBioMedicine 42 (2019) 311–325, https://doi.org/10.1016/j.ebiom.2019.03.045.
[14] Y. Ding, X. Chen, C. Liu, et al., Identification of a small molecule as inducer of ferroptosis and apoptosis through ubiquitination of GPX4 in triple negative breast cancer cells, J. Hematol. Oncol. 14 (1) (2021) 19, https://doi.org/10.1186/s13045-020-01016-8.
[15] A. Subramanian, P. Tamayo, V.K. Mootha, et al., Gene set enrichment analysis: a knowledge-based approach for interpreting genome-wide expression profiles, Proc. Natl. Acad. Sci. U. S. A. 102 (43) (2005) 15545–15550, https://doi.org/10.1073/pnas.0506580102.
[16] Y. Ye, Q. Dai, H. Qi, A novel defined pyroptosis-related gene signature for predicting the prognosis of ovarian cancer, Cell Death Dis. 7 (1) (2021) 71, https://doi.org/10.1038/s41420-021-00451-x.
[17] R. Zeng, S. Huang, X. Qiu, et al., Predicting the prognosis of esophageal adenocarcinoma by a pyroptosis-related gene signature, Front. Pharmacol. 12 (2021) 767187, https://doi.org/10.3389/fphar.2021.767187.
[18] M. Zhang, Y. Cheng, Z. Xue, Q. Sun, J. Zhang, A novel pyroptosis-related gene signature predicts the prognosis of glioma through immune infiltration, BMC Cancer 21 (1) (2021) 1311, https://doi.org/10.1186/s12885-021-09046-2.
[19] F. Chen, J. Yang, M. Fang, Y. Wu, D. Su, Y. Sheng, Necroptosis-related lncRNA to establish novel prognostic signature and predict the immunotherapy response in breast cancer, J. Clin. Lab. Anal. 36 (4) (2022) e24302, https://doi.org/10.1002/jcla.24302.
[20] L. Liu, Z. Tang, Y. Zeng, et al., Role of necroptosis in infection-related, immune-mediated, and autoimmune skin diseases, J. Dermatol. 48 (8) (2021) 1129–1138, https://doi.org/10.1111/1346-8138.15929.
[21] P. Tsvetkov, S. Coy, B. Petrova, et al., Copper induces cell death by targeting lipoylated TCA cycle proteins, Science 375 (6586) (2022) 1254–1261, https://doi.org/10.1126/science.abf0529.

[22] X. Liu, L. Nie, Y. Zhang, et al., Actin cytoskeleton vulnerability to disulfide stress mediates disulfidptosis, Nat. Cell Biol. 25 (3) (2023) 404–414, https://doi.org/10.1038/s41556-023-01091-2.

[23] B. Pal, Y. Chen, F. Vaillant, et al., A single-cell RNA expression atlas of normal, preneoplastic and tumorigenic states in the human breast, EMBO J. 40 (11) (2021) e107333, https://doi.org/10.15252/embj.2020107333.

[24] F. Quan, X. Liang, M. Cheng, et al., Annotation of cell types (ACT): a convenient web server for cell type annotation, Genome Med. 15 (1) (2023) 91, https://doi.org/10.1186/s13073-023-01249-5.

[25] L. Gong, D. Huang, Y. Shi, Z. Liang, H. Bu, Regulated cell death in cancer: from pathogenesis to treatment, Chin. Med. J. 136 (6) (2023) 653–665, https://doi.org/10.1097/CM9.0000000000002239.

[26] W. Gao, X. Wang, Y. Zhou, X. Wang, Y. Yu, Autophagy, ferroptosis, pyroptosis, and necroptosis in tumor immunotherapy, Signal Transduct. Targeted Ther. 7 (1) (2022) 196, https://doi.org/10.1038/s41392-022-01046-3.

[27] J. Deng, M. Zhou, T. Liao, et al., Targeting cancer cell ferroptosis to reverse immune checkpoint inhibitor therapy resistance, Front. Cell Dev. Biol. 10 (2022) 818453, https://doi.org/10.3389/fcell.2022.818453.

[28] A.B. Sarmento-Ribeiro, A. Scorilas, A.C. Gonçalves, T. Efferth, I.P. Trougakos, The emergence of drug resistance to targeted cancer therapies: clinical evidence, Drug Resist. Updates 47 (2019) 100646, https://doi.org/10.1016/j.drup.2019.100646.

[29] Q. Wu, W. Wu, B. Fu, L. Shi, X. Wang, K. Kuca, JNK signaling in cancer cell survival, Med. Res. Rev. 39 (6) (2019) 2082–2104, https://doi.org/10.1002/med.21574.

[30] D. Tang, R. Kang, T.V. Berghe, P. Vandenabeele, G. Kroemer, The molecular machinery of regulated cell death, Cell Res. 29 (5) (2019) 347–364, https://doi.org/10.1038/s41422-019-0164-5.

[31] K.K. Nyati, T. Kishimoto, The emerging role of Arid5a in cancer: a new target for tumors, Genes Dis 10 (3) (2022) 813–824, https://doi.org/10.1016/j.gendis.2021.12.012.

[32] J. Zhang, S. Hou, Z. You, et al., Expression and prognostic values of ARID family members in breast cancer, Aging (Albany NY) 13 (4) (2021) 5621–5637, https://doi.org/10.18632/aging.202489.

[33] L. Ivanciu, R.D. Gerard, H. Tang, F. Lupu, C. Lupu, Adenovirus-mediated expression of tissue factor pathway inhibitor-2 inhibits endothelial cell migration and angiogenesis, Arterioscler. Thromb. Vasc. Biol. 27 (2) (2007) 310–316, https://doi.org/10.1161/01.ATV.0000254147.89321, cf.

[34] W. Luo, X. Li, Z. Song, X. Zhu, S. Zhao, Long non-coding RNA AGAP2-AS1 exerts oncogenic properties in glioblastoma by epigenetically silencing TFPI2 through EZH2 and LSD1, Aging (Albany NY) 11 (11) (2019) 3811–3823, https://doi.org/10.18632/aging.102018.

[35] D. Zhao, J. Qiao, H. He, J. Song, S. Zhao, J. Yu, TFPI2 suppresses breast cancer progression through inhibiting TWIST-integrin α5 pathway, Mol. Med. 26 (1) (2020) 27, https://doi.org/10.1186/s10020-020-00158-2.

[36] P. Kempaiah, W. Kisiel, Human tissue factor pathway inhibitor-2 induces caspase-mediated apoptosis in a human fibrosarcoma cell line, Apoptosis 13 (5) (2008) 702–715, https://doi.org/10.1007/s10495-008-0207-8.

[37] S. Confalonieri, M. Quarto, G. Goisis, et al., Alterations of ubiquitin ligases in human cancer and their association with the natural history of the tumor, Oncogene 28 (33) (2009) 2959–2968, https://doi.org/10.1038/onc.2009.156.

[38] C.S. Wong, J. Sceneay, C.M. House, et al., Vascular normalization by loss of Siah2 results in increased chemotherapeutic efficacy, Cancer Res. 72 (7) (2012) 1694–1704, https://doi.org/10.1158/0008-5472.CAN-11-3310.

[39] M.G. Adam, S. Matt, S. Christian, et al., SIAH ubiquitin ligases regulate breast cancer cell migration and invasion independent of the oxygen status, Cell Cycle 14 (23) (2015) 3734–3747, https://doi.org/10.1080/15384101.2015.1104441.

[40] Z. Yang, S. Chen, H. Ying, W. Yao, Targeting syndecan-1: new opportunities in cancer therapy, Am. J. Physiol. Cell Physiol. 323 (1) (2022) C29–C45, https://doi.org/10.1152/ajpcell.00024.2022.

[41] T.L. Nguyen, W.E. Grizzle, K. Zhang, O. Hameed, G.P. Siegal, S. Wei, Syndecan-1 overexpression is associated with nonluminal subtypes and poor prognosis in advanced breast cancer, Am. J. Clin. Pathol. 140 (4) (2013) 468–474, https://doi.org/10.1309/AJCPZ1D8CALHDXCJ.

[42] M. Dong, X. Cui, G. Wang, Q. Zhang, X. Li, Development of a prognostic signature based on immune-related genes and the correlation with immune microenvironment in breast cancer, Aging (Albany NY) 14 (13) (2022) 5427–5448, https://doi.org/10.18632/aging.204158.

[43] S. Guo, X. Wu, T. Lei, et al., The role and therapeutic value of Syndecan-1 in cancer metastasis and drug resistance, Front. Cell Dev. Biol. 9 (2022) 784983, https://doi.org/10.3389/fcell.2021.784983.

[44] Y. Chen, L. Li, J. Zhang, Cell migration inducing hyaluronidase 1 (CEMIP) activates STAT3 pathway to facilitate cell proliferation and migration in breast cancer, J. Recept. Signal Transduct. Res. 41 (2) (2021) 145–152, https://doi.org/10.1080/10799893.2020.1800732.

[45] G. Rodrigues, A. Hoshino, C.M. Kenific, et al., Tumour exosomal CEMIP protein promotes cancer cell colonization in brain metastasis, Nat. Cell Biol. 21 (11) (2019) 1403–1412, https://doi.org/10.1038/s41556-019-0404-4.

[46] J. Xue, X. Zhu, X. Qiao, et al., CEMIP as a potential biomarker and therapeutic target for breast cancer patients, Int. J. Med. Sci. 19 (3) (2022) 434–445, https://doi.org/10.7150/ijms.58067.